

# Accelerated Imaginary-time Evolution Methods for the Computation of Solitary Waves

Jianke Yang and Taras I. Lakoba

Department of Mathematics and Statistics, University of Vermont, Burlington, VT 05401

Summary:

Two accelerated imaginary-time evolution methods are proposed for the computation of solitary waves in arbitrary spatial dimensions. For the first method (with traditional power normalization), the convergence conditions as well as conditions for optimal accelerations are derived. In addition, it is shown that for nodeless solitary waves, this method converges if and only if the solitary wave is linearly stable. The second method is similar to the first method except that it uses a novel amplitude normalization. The performance of these methods is illustrated on various examples. It is found that while the first method is competitive with the Petviashvili method, the second method delivers much better performance than the first method and the Petviashvili method.

## 1 Introduction

In the study of nonlinear wave equations, solitary waves play an important role. In certain cases (such as in integrable equations), solitary waves can be calculated analytically. But in a majority of other cases, analytical expressions for solitary waves are not available. Important examples which have arisen recently in the study of physical systems include optical solitary waves in periodic media [1, 2, 3] and nonlinear matter waves in Bose-Einstein condensates (see, e.g., [4, 5, 6]). In such cases, one relies on numerical techniques to determine the shapes of solitary waves. Several types of numerical methods have been proposed and used for this purpose, such as the Newton's iteration method [7, 8], the shooting method [9], the nonlinear Rayleigh-Ritz iteration method [10], the Petviashvili method [11, 12, 13, 14], the imaginary-time evolution method [4, 5, 6, 15, 16, 17], and the squared-operator iteration methods [18]. The imaginary-time evolution method is attractive for its simple implementation, insensitivity to the number of dimensions, and high accuracy (due to its compatibility with the pseudo-spectral method). In addition, if it converges, it usually does so faster than the squared-operator iteration methods.

The idea of the imaginary-time evolution method (ITEM) as applied to linear equations is quite old (see, e.g., [19, 20]). In the past decade, this method has also been applied to nonlinear equations [4, 5, 6, 15, 17]. In this method, one seeks the stationary solution of an evolution equation (usually, of the parabolic type) by numerically integrating that equation where time  $t$  is replaced by  $it$  (hence the name 'imaginary-time'), and normalizing the solution after each step of time integration to have a fixed  $L_2$  norm (called power by physicists). For linear equations, this method has long been known (see, e.g., [20]) to be equivalent to the problem of minimizing the energy functional of the physical system under the constraint that the solution being sought has a given power. Recently, this same

statement was shown to hold for nonlinear equations as well [17]. In [16], the authors treated the ITEM as a normalized gradient flow and proved its energy diminishing property. The ITEM, in its original form, is quite slow. In addition, it does not always converge to a stationary solution even if the initial function is quite close to the solution. In an effort to improve the convergence rate of the ITEM, the authors of Ref. [15] demonstrated that if the Sobolev gradients are used in the minimization of the energy functional, the convergence of the ITEM can be greatly accelerated (an equivalent possibility was mentioned in passing in [20], although no related details were provided there.) Alternatively, the authors of [17] used the steepest descent technique in the minimization of the energy functional and achieved fast convergence as well. However, these earlier studies or applications of the ITEM did not consider the conditions under which the ITEM and its accelerated versions would converge. So it was not clear when those methods could be used. In addition, the important practical question of establishing the conditions for the optimal acceleration of the ITEM was not considered either.

An important question in the studies of solitary waves is their linear stability [21, 22, 23, 24, 25]. Most numerical techniques used to find solitary waves, such as the Newton's iteration method, the shooting method, and the Petviashvili method, yield no information about the stability of the solitary wave being obtained [7, 9, 12]. A remarkable fact about the ITEM and its properly accelerated version (with the usual power normalization), as we will show in this paper, is that the convergence of this numerical method is directly related to the linear stability of the corresponding solitary wave, provided that this wave is nodeless. This means that both existence and linear stability of these solitary waves can be obtained by this single numerical procedure.

In this paper, we propose two new accelerated ITEMS for the computation of solitary waves in general nonlinear wave equations. Our acceleration technique is to introduce an acceleration operator to the imaginary-time equation, analogous to the preconditioning technique for solving systems of linear equations. For the first method, which uses power normalization, three important theoretical results are derived. One result is that convergence conditions of this method are explicitly obtained. This puts the application of this method on a solid theoretical footing. These convergence conditions show that in most cases, this method converges when the underlying solitary wave is nodeless, but there also exist cases when the method converges to solitary waves with nodes. Another result is that for nodeless solitary waves, this method converges if and only if the solitary wave is linearly stable. This connection between convergence of this method and linear stability of the underlying solitary wave is a novel property of this numerical method which has not been seen in other schemes. The third result is that explicit conditions for optimal acceleration of this method are obtained. These results provide the optimal practical implementation of this accelerated ITEM. The performance of this method is illustrated on various examples, and it is found to be competitive with the Petviashvili method. The second accelerated ITEM which we propose is similar to the first method except that it uses a non-traditional amplitude normalization. We will show through examples that this second method delivers better performance than the first method and the Petviashvili method.

This paper is structured as follows. In Sec. 2, we introduce the original imaginary-time evolution method. In Sec. 3, we propose the first accelerated imaginary-time evolution method and derive its convergence conditions. In Sec. 4, we show that for nodeless solitary waves, the convergence of this

first method is directly linked to the linear stability of the solitary wave. In Sec. 5, we establish explicit conditions for the optimal acceleration of the first method. In Sec. 6, we propose the second accelerated imaginary-time evolution method, which employs the amplitude normalization. In Sec. 7, we apply both methods as well as the Petviashvili method to several examples, and show that the second accelerated imaginary-time evolution method delivers the best performance, while the first method is comparable to the Petviashvili method in performance. Sec. 8 concludes the paper. In the appendix, we attach a matlab code for one of the examples.

## 2 Preliminaries on the original imaginary-time evolution method

The problem we are interested in is the numerical determination of solitary waves in general scalar nonlinear wave equations in arbitrary spatial dimensions. To maintain the focus of the presentation, we first develop the theory for the  $N$ -dimensional generalized nonlinear Schrödinger equation with an arbitrary potential. The extension of this theory to more general scalar nonlinear wave equations will be presented at the end of Sec. 5.

The  $N$ -dimensional generalized nonlinear Schrödinger equation with an arbitrary potential has the following form:

$$iU_t + \nabla^2 U + F(|U|^2, \mathbf{x})U = 0, \quad (1)$$

where  $\mathbf{x} = (x_1, x_2, \dots, x_N)$  is a  $N$ -dimensional spatial variable,

$$\nabla^2 = \frac{\partial^2}{\partial x_1^2} + \frac{\partial^2}{\partial x_2^2} + \dots + \frac{\partial^2}{\partial x_N^2} \quad (2)$$

is the  $N$ -dimensional Laplacian, and  $F(.,.)$  is a real-valued function. This system is Hamiltonian. Solitary waves of Eq. (1) are sought in the form

$$U(\mathbf{x}, t) = u(\mathbf{x})e^{i\mu t}, \quad (3)$$

where  $u(\mathbf{x})$  is a real-valued, localized function, and  $\mu$  is a real parameter called the propagation constant. Then, from Eqs. (1) and (3), function  $u(\mathbf{x})$  is found to satisfy the equation

$$L_{00}u = \mu u, \quad (4)$$

where

$$L_{00} \equiv \nabla^2 + F(u^2, \mathbf{x}). \quad (5)$$

Equation (4) admits solitary waves for a large class of functions  $F(u^2, \mathbf{x})$  [26, 27]. In this paper, we always assume that the solitary wave we are trying to obtain numerically does exist.

In the original imaginary-time evolution method, one numerically integrates the equation

$$u_t = L_{00}u, \quad (6)$$

which is obtained from Eq. (1) by replacing  $t$  with  $it$  (hence the name ‘imaginary-time’), and then normalizes the solution after each step of time integration to have a fixed power. The power  $P$  of the solitary wave  $u(\mathbf{x})$  is defined as

$$P(\mu) = \int_{-\infty}^{\infty} u^2(\mathbf{x}; \mu) d\mathbf{x}. \quad (7)$$

The simplest implementation of numerical time integration is to use the Euler method, whereby the ITEM scheme is:

$$u_{n+1} = \left[ \frac{P}{\langle \hat{u}_{n+1}, \hat{u}_{n+1} \rangle} \right]^{\frac{1}{2}} \hat{u}_{n+1}, \quad (8)$$

and

$$\hat{u}_{n+1} = u_n + [L_{00}u]_{u=u_n} \Delta t. \quad (9)$$

Here  $u_n$  is the solution after the  $n$ th iteration,

$$\langle f, g \rangle = \int_{-\infty}^{\infty} f(\mathbf{x})^* g(\mathbf{x}) d\mathbf{x} \quad (10)$$

is the standard inner product in the  $N$ -dimensional space of square-integrable functions, and the superscript “\*” represents complex conjugation. Note that step (8) of the ITEM scheme guarantees that the power at every iteration is conserved:

$$\langle u_n, u_n \rangle = P, \quad n = 1, 2, \dots \quad (11)$$

Thus, if iterations (8)-(9) converge to a solitary wave  $u(\mathbf{x})$ , then this  $u(\mathbf{x})$  must satisfy Eq. (4), with its power being  $P$  and the propagation constant  $\mu$  being equal to

$$\mu = \frac{1}{P} \langle L_{00}u, u \rangle. \quad (12)$$

In the following sections, we will use two linear operators, whose explicit forms are given by the following definition.

**Definition 1** Operators  $L_0$  and  $L_1$  are defined as

$$L_0 \equiv L_{00} - \mu = \nabla^2 + F(u^2, \mathbf{x}) - \mu, \quad (13)$$

and

$$L_1 \equiv \nabla^2 + F(u^2, \mathbf{x}) + 2u^2 F_{u^2}(u^2, \mathbf{x}) - \mu, \quad (14)$$

where  $F_{u^2} \equiv \partial F / \partial u^2$ .

Under these notations,  $L_0 u = 0$ , and  $L_1$  is the linearization operator of  $L_0 u$  with respect to  $u$ .

### 3 An accelerated imaginary-time evolution method

A major drawback of the original ITEM (8)-(9) is that its convergence is quite slow, because the time step  $\Delta t$  has to be very small in order for it to converge (see Note 1 below for explanation). To overcome this difficulty, one idea is to use implicit time-stepping methods (such as the backward Euler method) to solve the imaginary-time equation (6) (see, e.g., [16]). Implicit methods allow larger time steps without causing divergence to the iterations. However, for nonlinear equations or in high dimensions, implicit schemes are difficult to implement, and their accuracies are often low (if finite-difference discretization is used). Another idea of accelerating the ITEM (see [15]) is to use the Sobolev gradients in the minimization of the energy functional. This idea is analogous to the preconditioning technique applied to the imaginary-time equation (6). Below we will extend this idea and propose a new accelerated ITEM that is explicit but fast-converging.

In our accelerated ITEM, instead of evolving the original imaginary-time equation (6), we evolve the following “pre-conditioned” imaginary-time equation

$$u_t = M^{-1} [L_{00}u - \mu u], \quad (15)$$

where  $M$  is a positive-definite and self-adjoint “preconditioning” operator. The stationary solution of this equation is still  $u(\mathbf{x})$ . Applying the Euler method to this new equation, the new accelerated ITEM method (AITEM) we propose is:

$$u_{n+1} = \hat{u}_{n+1} \sqrt{\frac{P}{\langle \hat{u}_{n+1}, \hat{u}_{n+1} \rangle}}, \quad (16)$$

$$\hat{u}_{n+1} = u_n + M^{-1} (L_{00}u - \mu u)_{u=u_n, \mu=\mu_n} \Delta t, \quad (17)$$

and

$$\mu_n = \frac{\langle L_{00}u, M^{-1}u \rangle}{\langle u, M^{-1}u \rangle} \Big|_{u=u_n}, \quad (18)$$

where  $P$  is the power defined in Eq. (7), which is pre-specified. Notice that our updating formula (18) for  $\mu_n$  is quite special, different from the usual formula (12). This special updating formula (18) enables us to derive the convergence properties of the above AITEM, which we will do in this section. If  $M$  is the identity operator, then the above scheme is closely related to the original ITEM (8)-(9), and both have similar (slow) convergence properties. But if  $M$  takes other sensible forms [such as (45) below], convergence of the above AITEM will be much faster. In this paper, we will call  $M$  the acceleration operator.

Before discussing the convergence conditions of the AITEM (16)-(18), we first present an example to demonstrate the drastic improvement in convergence of the AITEM (16)-(18) over that of the ITEM (8)-(9).

**Example 1** The nonlinear Schrödinger equation in one spatial dimension,

$$u_{xx} + u^3 = \mu u \quad (19)$$

admits the solitary wave

$$u(x) = \sqrt{2} \operatorname{sech} x \quad (20)$$

with  $P = 4$  and  $\mu = 1$ . To apply the AITEM for this solution, we take  $M = 1 - \partial_{xx}$ ,  $\Delta t = 1.5$ , and the Gaussian initial condition  $u_0(x) = e^{-x^2}$ . The  $x$ -interval is taken to be  $[-15, 15]$ , discretized by 128 grid points, and the discrete Fourier transform is used to calculate  $u_{xx}$  and to invert operator  $M$ . For the ITEM, the scheme parameters are the same, except that  $\Delta t = 0.01$  (when  $\Delta t > 0.011$ , the ITEM diverges). Defining the error as the  $L_2$  norm of the solution difference between successive iterations, i.e.  $[\int (u_n - u_{n-1})^2 dx]^{1/2}$ , we find that for the error to drop below  $10^{-10}$ , the AITEM and ITEM take, respectively, 33 and 2160 iterations. Thus, the AITEM for this case is about two orders of magnitude faster than the original ITEM. The main reason for this drastic improvement of convergence is that for the AITEM, the time step  $\Delta t$  can be taken much larger (which is 1.5 above) without causing divergence. This is made possible by the introduction of the acceleration operator  $M$ .

Now we derive the convergence conditions for the AITEM (16)-(18). To do so, we introduce the following assumption on the kernel of  $L_1$  which holds in generic cases (in rare cases, this assumption may break down, see Fig. 7 in [28]).

**Assumption 1** *If function  $F$  in Eq. (4) does not depend explicitly on certain spatial coordinates  $\{x_{j_1}, x_{j_2}, \dots, x_{j_k}\}$  ( $1 \leq j_1, j_2, \dots, j_k \leq N$ ), we assume that the only eigenfunctions in the kernel of  $L_1$  that are orthogonal to  $u(\mathbf{x})$  are the  $k$  translational-invariance modes  $\partial u / \partial x_{j_s}(\mathbf{x})$ ,  $1 \leq s \leq k$ .*

We also introduce a notation: for any operator  $L$ , we denote the number of its positive eigenvalues as  $p(L)$ .

Under the above assumption and notation, we have the following theorem on the convergence of the AITEM (16)-(18).

**Theorem 1** *Let Assumption 1 be valid. Define  $\Delta t_{\max} = -2/\Lambda_{\min}$ , where  $\Lambda_{\min}$  is the minimum (negative) eigenvalue of operator  $\mathcal{L}$  in Eq. (24). Then if  $\Delta t > \Delta t_{\max}$ , the AITEM (16)-(18) diverges. If  $\Delta t < \Delta t_{\max}$ , the following convergence statements on this AITEM hold.*

1. *If  $p(L_1) = 0$  and  $P'(\mu) \neq 0$ , then the AITEM converges.*
2. *Suppose  $p(L_1) = 1$ , then  $p(M^{-1}L_1) = 1$ . Denote the eigenfunction of this single positive eigenvalue of  $M^{-1}L_1$  as  $\psi(\mathbf{x})$ . Then if  $\langle \psi, u \rangle \neq 0$ , the AITEM converges for  $P'(\mu) > 0$  and diverges for  $P'(\mu) < 0$ . If, however,  $\langle \psi, u \rangle = 0$ , the AITEM diverges.*
3. *If  $p(L_1) > 1$ , the AITEM diverges.*

**Proof** To analyze the convergence properties of the AITEM (16)-(18), we use the linearization technique. Let

$$u_n = u + \tilde{u}_n, \quad |\tilde{u}_n| \ll |u|, \quad (21)$$

where  $\tilde{u}_n(\mathbf{x})$  is the error. When this equation is substituted into the power-normalization step (16) and only terms of  $O(\tilde{u}_n)$  retained, one obtains that the error is orthogonal to  $u(\mathbf{x})$ :

$$\langle \tilde{u}_n, u \rangle = 0, \quad \text{for all } n. \quad (22)$$

Substituting Eq. (21) into (17)-(18) and linearizing, we find that the error satisfies the following iteration equation

$$\tilde{u}_{n+1} = (1 + \Delta t \mathcal{L}) \tilde{u}_n, \quad (23)$$

where operator  $\mathcal{L}$  is

$$\mathcal{L}\Psi = M^{-1} \left( L_1 \Psi - \frac{\langle L_1 \Psi, M^{-1} u \rangle}{\langle u, M^{-1} u \rangle} u \right). \quad (24)$$

Convergence of the AITEM depends on the eigenvalues of operator  $\mathcal{L}$ . In view of the orthogonality constraint (22), the eigenvalue problem for  $\mathcal{L}$  that we need to consider is

$$\mathcal{L}\Psi = \Lambda \Psi, \quad \Psi \in S, \quad (25)$$

where

$$S = \{\Psi(\mathbf{x}) : \langle \Psi, u \rangle = 0\}. \quad (26)$$

Note that when  $\Lambda \neq 0$ , by taking the inner product between equation  $\mathcal{L}\Psi = \Lambda \Psi$  and  $u$ , one easily gets  $\langle \Psi, u \rangle = 0$ , i.e.  $\Psi \in S$ . Thus  $\Psi \in S$  in Eq. (25) constitutes a constraint only for zero eigenvalues of  $\mathcal{L}$ . As we will show below, all eigenvalues  $\Lambda$  of  $\mathcal{L}$  are real, and all eigenfunctions of  $\mathcal{L}$  form a complete set in  $S$ . Thus, in view of Assumption 1, the necessary and sufficient conditions for the AITEM to converge are that (i) for all non-zero eigenvalues  $\Lambda$  of  $\mathcal{L}$ ,

$$-1 < 1 + \Lambda \Delta t < 1; \quad (27)$$

(ii) for the zero eigenvalue of Eq. (25) (if exists), its eigenfunctions must be translational-invariance eigenmodes  $u_{x_j}$  (which lead to a spatially translated solitary wave of Eq. (4) and do not affect the convergence of iterations). If  $\Delta t > \Delta t_{max}$  with  $\Delta t_{max}$  given in Theorem 1, then the left inequality in (27) is not met, thus the AITEM diverges. If  $\Delta t < \Delta t_{max}$ , the left inequality in (27) is satisfied, hence we only need to consider the right inequality in (27), and the second condition (ii).

We consider the condition (ii) first. Suppose Eq. (25) has a zero eigenvalue with eigenfunction  $\Psi(\mathbf{x})$ , i.e.,

$$L_1 \Psi - \frac{\langle L_1 \Psi, M^{-1} u \rangle}{\langle u, M^{-1} u \rangle} u = 0, \quad \Psi \in S. \quad (28)$$

Differentiating Eq. (4) with respect to parameter  $\mu$ , we find that

$$L_1 u_\mu = u. \quad (29)$$

Hence the solution  $\Psi$  of Eq. (28) is  $\alpha u_\mu$ , where  $\alpha$  is a constant, plus functions in the kernel of  $L_1$ . In view of Assumption 1 on the kernel of  $L_1$ , we see that  $\langle \Psi, u \rangle = \alpha \langle u_\mu, u \rangle = \alpha P'(\mu)/2$ . Thus if  $P'(\mu) \neq 0$ , then in order for  $\Psi \in S$ ,  $\alpha$  must be zero, hence  $\Psi$  is in the kernel of  $L_1$ . According to Assumption 1,  $\Psi$  then must be a translational-invariance eigenmode which does not affect the convergence of iterations.

Next we consider the right inequality in (27), which is simply  $\Lambda < 0$ . We will analyze when this condition is met. To facilitate the analysis, we introduce the following new variables and operators

$$\hat{\Psi} = M^{1/2}\Psi, \quad \hat{u} = M^{-1/2}u, \quad \hat{L}_1 = M^{-1/2}L_1M^{-1/2}. \quad (30)$$

Then the eigenvalue problem (25) becomes the following equivalent one with eigenvalues unchanged:

$$\hat{\mathcal{L}}\hat{\Psi} = \Lambda\hat{\Psi}, \quad \hat{\Psi} \in \hat{S}, \quad (31)$$

where

$$\hat{\mathcal{L}}\hat{\Psi} = \hat{L}_1\hat{\Psi} - \hat{H}\hat{u}, \quad \hat{H} = \frac{\langle \hat{L}_1\hat{\Psi}, \hat{u} \rangle}{\langle \hat{u}, \hat{u} \rangle}, \quad (32)$$

and

$$\hat{S} = \{\hat{\Psi}(\mathbf{x}) : \langle \hat{\Psi}, \hat{u} \rangle = 0\}. \quad (33)$$

It is easy to see that operator  $\hat{\mathcal{L}}$  is self-adjoint in the set  $\hat{S}$  due to  $L_1$  and  $M$  being self-adjoint and  $M$  being positive definite. Thus all eigenvalues  $\Lambda$  of  $\hat{\mathcal{L}}$  are real, and all eigenfunctions  $\hat{\Psi}$  of  $\hat{\mathcal{L}}$  form a complete set in  $\hat{S}$ . As a result, all eigenvalues  $\Lambda$  of  $\mathcal{L}$  are real, and all eigenfunctions of  $\mathcal{L}$  form a complete set in  $S$ . In addition, since  $\hat{L}_1$  is similar to  $M^{-1}L_1$  and in view of the *Sylvester inertia law* (see, e.g., Theorems 4.5.8 and 7.6.3 in [29]),  $p(\hat{L}_1) = p(M^{-1}L_1) = p(L_1)$ .

The eigenvalue problem (31) is equivalent to the one arising in the linear stability analysis of nodeless solitary waves (see, e.g., [2, 21] and, in particular, Eq. (2.3.9) in [2]), and has been well studied. To determine the sign of eigenvalue  $\Lambda$ , we expand  $\hat{\Psi}$  into the complete set of eigenfunctions of the self-adjoint operator  $\hat{L}_1$  as

$$\hat{\Psi}(\mathbf{x}) = \sum_k b_k \hat{\psi}_k(\mathbf{x}) + \int_I b(\lambda) \hat{\psi}(\mathbf{x}; \lambda) d\lambda, \quad (34)$$

where  $\hat{\psi}_k(\mathbf{x})$  and  $\hat{\psi}(\mathbf{x}; \lambda)$  are the properly normalized discrete and continuous eigenfunctions of  $\hat{L}_1$  with eigenvalues  $\lambda_k$  and  $\lambda$ . The coefficients in Eq. (34) are given by  $b_k = \langle \hat{\psi}_k, \hat{\Psi} \rangle$  and  $b = \langle \hat{\psi}, \hat{\Psi} \rangle$ . Function  $\hat{u}$  can be expanded in a similar way with coefficients  $c_k = \langle \hat{\psi}_k, \hat{u} \rangle$  and  $c(\lambda) = \langle \hat{\psi}, \hat{u} \rangle$ . When  $\hat{H} = 0$ , the analysis is trivial and the convergence conditions in Theorem 1 can be easily obtained. Thus we only consider the  $\hat{H} \neq 0$  case below. In this case, substituting expansions of  $\hat{u}$  and  $\hat{\Psi}$  into Eq. (31), one finds that  $b_k = \hat{H}c_k/(\lambda_k - \Lambda)$ ,  $b(\lambda) = \hat{H}c(\lambda)/(\lambda - \Lambda)$ . Substituting these relations into the orthogonality condition  $\langle \hat{\Psi}, \hat{u} \rangle = 0$ , we get

$$Q(\Lambda) \equiv \sum_k \frac{|c_k|^2}{\lambda_k - \Lambda} + \int_I \frac{|c(\lambda)|^2}{\lambda - \Lambda} d\lambda = 0. \quad (35)$$

If  $p(L_1) = p(\hat{L}_1) = 0$ , i.e. all eigenvalues of  $\hat{L}_1$  are negative, then  $Q(\Lambda)$  does not change sign when  $\Lambda > 0$ , hence equation (35) has no positive roots, and the right inequality in (27) is met. We have shown above that when  $P'(\mu) \neq 0$ , condition (ii) is met also, thus the AITEM converges. If  $p(L_1) = p(\hat{L}_1) > 1$ , denote  $\hat{L}_1$ 's two positive eigenvalues as  $\lambda_1$  and  $\lambda_2$ . If the corresponding expansion coefficients  $c_1$  and  $c_2$  in  $\hat{u}$  are such that  $c_1c_2 \neq 0$ , then since  $Q(\Lambda)$  is continuous and monotonic in the interval  $(\lambda_1, \lambda_2)$ , and it approaches  $-\infty$  and  $\infty$  at the two ends of this interval,  $Q(\Lambda)$  obviously has a positive root between  $\lambda_1$  and  $\lambda_2$ , hence the right inequality in (27) is not met,



and the AITEM diverges. If  $c_k = 0$  ( $k = 1$  or  $2$ ), then  $\Lambda = \lambda_k > 0$  is an eigenvalue of Eq. (31) with  $\hat{\Psi} = \hat{\psi}_k$ , hence the AITEM also diverges.

Now we consider the case  $p(L_1) = p(\hat{L}_1) = 1$ . Denote this single positive eigenvalue of  $\hat{L}_1$  as  $\lambda_1$ , and its eigenfunction as  $\hat{\psi}$ . If  $\langle \hat{\psi}, \hat{u} \rangle = 0$ , then  $\Lambda = \lambda_1 > 0$  is an eigenvalue of Eq. (31) with  $\hat{\Psi} = \hat{\psi}$ , hence the AITEM diverges. Below we consider the  $\langle \hat{\psi}, \hat{u} \rangle \neq 0$  case. Clearly  $Q(\Lambda)$  cannot have zeros when  $\Lambda > \lambda_1$ . Whether  $Q(\Lambda)$  has a positive zero in  $(0, \lambda_1)$  depends on the sign of  $Q(0)/\hat{H}$ : if  $Q(0)/\hat{H} < 0$ , then  $Q(\lambda)$  has a positive zero, and vice versa. From Eqs. (31) and (32), we see that  $Q(0)/\hat{H} = \langle \hat{L}_1^{-1} \hat{u}, \hat{u} \rangle$ . In view of Eq. (30), it follows that  $Q(0)/\hat{H} = \langle L_1^{-1} u, u \rangle$ . Then from Eq. (29), we get  $Q(0)/\hat{H} = P'(\mu)/2$ . Consequently, if  $P'(\mu) > 0$ , the right inequality in (27) is met, and the AITEM converges; if  $P'(\mu) < 0$ , the AITEM diverges. Lastly, we notice from Eq. (30) that when  $\hat{\psi}$  is an eigenfunction of  $\hat{L}_1$ ,  $\psi = M^{-1/2} \hat{\psi}$  is an eigenfunction of  $M^{-1} L_1$  at the same eigenvalue, thus  $\langle \hat{\psi}, \hat{u} \rangle = \langle \psi, u \rangle$ . This completes the proof of Theorem 1.  $\square$

**Note 1** If  $M$  is taken as the identity operator, then our AITEM (16)-(18) becomes similar to the original ITEM (8)-(9). In this case, the smallest eigenvalue of  $\mathcal{L}$  is  $\Lambda_{min} = -\infty$ , which leads to  $\Delta t_{max} = 0$ . However, in any computer implementation of this method, space is discretized. For the discretized operator of  $\mathcal{L}$ ,  $\Lambda_{min}$  is finite, not  $-\infty$ , thus  $\Delta t_{max} > 0$ , hence this method (as well as the original ITEM) can still be used (see Example 1). But for any accurate spatial discretizations,  $\Lambda_{min}$  is large negative, hence  $\Delta t_{max}$  is very small, which results in the slow convergence of this method and the original ITEM. For a more sensible choice of  $M$  such as (45) below, the smallest eigenvalues of  $\mathcal{L}$  and its discretized version are both  $O(1)$  and almost identical. This makes  $\Delta t_{max}$  much larger, hence the AITEM (16)-(18) converges much faster (see Example 1).

Theorem 1 is one of the main results of this article. It puts the application of the AITEM (16)-(18) on a firm theoretical basis. A corollary of this theorem can be readily established below.

**Corollary 1** Consider Eq. (4) with  $\lim_{|\mathbf{x}| \rightarrow \infty} F(0, \mathbf{x}) = 0$ . Under Assumption 1 and restriction  $\Delta t < \Delta t_{max}$ , where  $\Delta t_{max}$  is given in Theorem 1, the AITEM (16)-(18) diverges if the solitary wave  $u(\mathbf{x})$  has nodes (where  $u(\mathbf{x}) = 0$ ) and  $F_{u^2}(u^2, \mathbf{x}) \geq 0$  for all  $\mathbf{x}$ ; if  $u(\mathbf{x})$  is nodeless and  $F_{u^2}(u^2, \mathbf{x}) \leq 0$  for all  $\mathbf{x}$ , then the AITEM converges.

To prove this corollary, we need the following lemma.

**Lemma 1** Consider the  $N$ -dimensional, linear Schrödinger eigenvalue problem

$$\nabla^2 \psi - V(\mathbf{x})\psi = \lambda\psi, \quad (36)$$

where  $V(\mathbf{x}) \rightarrow 0$  as  $|\mathbf{x}| \rightarrow \infty$ . Let its discrete eigenvalues be arranged in the decreasing order:  $\lambda_1 > \lambda_2 \geq \dots \geq \lambda_m > 0$ , with the continuous spectrum being at  $\lambda < 0$ . Let  $V_1(\mathbf{x})$  and  $V_2(\mathbf{x})$  be two potentials such that  $V_2(\mathbf{x}) \leq V_1(\mathbf{x})$  for all  $\mathbf{x}$ , and  $V_2(\mathbf{x}) \not\equiv V_1(\mathbf{x})$ . Then the discrete eigenvalues  $\{\lambda_k^{(2)}\}$  of Eq. (36) with potential  $V_2$  are larger than the corresponding eigenvalues  $\{\lambda_k^{(1)}\}$  of the same equation with potential  $V_1$ , i.e.,  $\lambda_k^{(2)} > \lambda_k^{(1)}$ ,  $k = 1, 2, \dots$

This lemma says that deepening the potential (making  $V(\mathbf{x})$  larger) shifts the eigenvalues of Eq. (36) downward.

**Proof of Lemma 1:** Define the potential function

$$V(\mathbf{x}; \alpha) = V_1(\mathbf{x}) + \alpha[V_2(\mathbf{x}) - V_1(\mathbf{x})], \quad (37)$$

where  $\alpha$  is a real parameter. As  $\alpha$  increases from 0 to 1,  $V(\mathbf{x}; \alpha)$  changes from  $V_1(\mathbf{x})$  to  $V_2(\mathbf{x})$ . We now analyze how a discrete eigenvalue  $\lambda$  of Eq. (36) changes as  $\alpha$  continuously varies. For this purpose, we differentiate Eq. (36) with respect to  $\alpha$ , and obtain

$$\left(\nabla^2 - V - \lambda\right) \frac{\partial \psi}{\partial \alpha} = \frac{d\lambda}{d\alpha} \psi + (V_2 - V_1) \psi. \quad (38)$$

In order for this equation to have a localized solution  $\partial \psi / \partial \alpha$ , its right-hand side must be orthogonal to the homogeneous solution  $\psi(\mathbf{x}; \alpha)$ . This yields the relation

$$\frac{d\lambda}{d\alpha} = \frac{\langle (V_1 - V_2) \psi, \psi \rangle}{\langle \psi, \psi \rangle}. \quad (39)$$

According to our assumption,  $V_2(\mathbf{x}) \leq V_1(\mathbf{x})$  for all  $\mathbf{x}$ , and  $V_2(\mathbf{x}) \neq V_1(\mathbf{x})$ ; thus  $d\lambda/d\alpha > 0$ . This means that  $\lambda_k^{(2)} > \lambda_k^{(1)}$ ,  $k = 1, 2, \dots$ . Hence Lemma 1 is proved.  $\square$

With this lemma, we now prove Corollary 1.

**Proof of Corollary 1:** First, we recall the definitions of the two operators  $L_0$  and  $L_1$  in Eqs. (13) and (14), and the fact of  $L_0 u(\mathbf{x}) = 0$ , i.e.,  $L_0$  has a zero eigenvalue  $\lambda_a = 0$  with eigenfunction  $u(\mathbf{x})$ . We will also use a well known result about linear Schrödinger operators, which says that the largest eigenvalue of those operators is simple and the corresponding eigenfunction is nodeless [30]. We now consider two possibilities in regards to the nodes of  $u(\mathbf{x})$ .

(1) Suppose  $u(\mathbf{x})$  has at least one node. Then, by the aforementioned property of linear Schrödinger operators,  $L_0$  must also have at least one positive eigenvalue  $\lambda_b > 0$  whose eigenfunction is nodeless. Comparing the two Schrödinger operators  $L_0$  and  $L_1$ , we see that the difference in their potentials is  $2u^2 F_{u^2}(u^2, \mathbf{x})$ . If  $F_{u^2}(u^2, \mathbf{x}) \geq 0$  and  $F_{u^2}(u^2, \mathbf{x}) \not\equiv 0$ , then it is seen from Lemma 1 that operator  $L_1$  must have at least two positive eigenvalues corresponding to the eigenvalues  $\lambda_a$  and  $\lambda_b$  of  $L_0$ . Hence according to Theorem 1, the AITEM diverges.

(2) If  $u(\mathbf{x})$  is nodeless, then zero is the largest eigenvalue of  $L_0$ . When  $F_{u^2}(u^2, \mathbf{x}) \leq 0$  and  $F_{u^2}(u^2, \mathbf{x}) \not\equiv 0$ , then by Lemma 1, the eigenvalues of  $L_1$  are all negative. Thus according to Theorem 1, the AITEM converges. This completes the proof of Corollary 1.  $\square$

Corollary 1 can be readily used on certain equations, and two examples are shown below.

1. Consider the focusing nonlinear Schrödinger equation with a single-well potential:

$$u_{xx} + 6\text{sech}^2 x u + u^3 = \mu u. \quad (40)$$

This equation admits a family of solitary waves with nodes [see an example in Fig. 1(a)]. Here  $F_{u^2}(u^2, \mathbf{x}) = 1 > 0$ , thus according to Corollary 1, the AITEM diverges for these solutions, which we have confirmed numerically.

2. Consider the defocusing nonlinear Schrödinger equation with a single-well potential:

$$u_{xx} + 6\text{sech}^2 x u - u^3 = \mu u. \quad (41)$$

This equation admits a family of nodeless solitary waves [see an example in Fig. 1(b)]. Here  $F_{u^2}(u^2, \mathbf{x}) = -1 < 0$ , thus according to Corollary 1, the AITEM converges for these solutions under restriction  $\Delta t < \Delta t_{max}$  (even though it can be verified that  $P'(\mu) < 0$  here).

Corollary 1 suggests that the AITEM tends to diverge for solitary waves with nodes (such solutions are often called “excited states”). Indeed, this is often the case. However, there are examples where the AITEM *converges* for solitary waves with nodes. This could occur if all the eigenvalues of  $L_1$  are negative. For a solitary wave  $u(\mathbf{x})$  with nodes, since  $L_0 u = 0$ ,  $L_0$  must also have positive eigenvalues [30]. But if  $F_{u^2}(u^2, \mathbf{x}) \leq 0$  for all  $\mathbf{x}$ , then the eigenvalues of  $L_1$  are lower than those of  $L_0$  according to Lemma 1. If the potential difference  $|2u^2 F_{u^2}(u^2, \mathbf{x})|$  between  $L_0$  and  $L_1$  is large enough, it is possible for all the eigenvalues of  $L_1$  to be pushed below zero, resulting in the convergence of the AITEM. One such example is given below.

**Example 2** Consider the defocusing nonlinear Schrödinger equation with a double-well potential:

$$u_{xx} + 6 \left[ \text{sech}^2(x+1) + \text{sech}^2(x-1) \right] u - u^3 = \mu u. \quad (42)$$

For this equation,  $F_{u^2}(u^2, x) = -1 < 0$ . This equation admits a family of single-node solitary waves, whose power curve is displayed in Fig. 2(a). It is seen that  $P'(\mu) < 0$  for the entire family. Two representative solutions with powers  $P = 3$  and  $P = 10$  are displayed in Fig. 2(b). The spectra of operator  $L_1$  for these two waves are plotted in Fig. 2(c, d), respectively. At the lower power  $P = 3$ ,  $p(L_1) = 1$ . However, at the higher power  $P = 10$ ,  $|2u^2 F_{u^2}(u^2, \mathbf{x})| = 2u^2$  is large enough such that  $p(L_1) = 0$ , hence according to Theorem 1, the AITEM converges.

## 4 Connection between convergence and linear stability

The convergence theorem 1 strongly resembles the linear stability conditions of nodeless solitary waves in the generalized NLS equations (1) [2, 21, 23, 24, 31]. For such solitary waves, the following stability conditions have been established [2]:

*For a nodeless solitary wave in Eq. (1), (i) if  $p(L_1) < 0$ , the wave is linearly stable; (ii) if  $p(L_1) = 1$ , the wave is linearly stable if  $P'(\mu) > 0$  and unstable if  $P'(\mu) < 0$ ; (iii) if  $p(L_1) > 1$ , the wave is linearly unstable.*

This stability result is almost identical to our convergence theorem 1, indicating that the AITEM (16)-(18) usually converges to a nodeless solitary wave if and only if this wave is linearly stable.

The only notable difference between the above stability and convergence results is in the case of  $p(L_1) = 1$ , where the convergence theorem has a condition on  $\langle \psi, u \rangle$  which is absent in the stability theorem. However, for nodeless solitary waves  $u(\mathbf{x})$  with  $p(L_1) = 1$ , condition  $\langle \psi, u \rangle \neq 0$  in Theorem 1 is met in generic cases, thus the stability and convergence results are the same for this case as well. For the following two choices of the acceleration operator  $M$ , we can actually show that condition  $\langle \psi, u \rangle \neq 0$  is strictly satisfied.

The first choice is when  $M$  is the identity operator, where the AITEM becomes similar to the original ITEM (8)-(9). In this case, if  $p(L_1) = 1$ , then  $\psi(\mathbf{x})$  is the eigenfunction of the largest eigenvalue of the Schrödinger operator  $L_1$ , which is known to be nodeless [30]. Since  $u(\mathbf{x})$  is nodeless as well,  $\langle \psi, u \rangle$  thus is non-zero.

The second choice is a very practical one,  $M = \mu - \nabla^2$ , which will be shown to yield optimal acceleration for a large class of equations in the next section. For this  $M$ , the eigenvalue equation  $M^{-1}L_1\psi = \lambda\psi$  can be rewritten as the following Schrödinger equation

$$\nabla^2\psi - \mu\psi + \frac{\mathcal{V}(\mathbf{x})}{1+\lambda}\psi = 0, \quad (43)$$

where

$$\mathcal{V}(\mathbf{x}) = F(u^2, \mathbf{x}) + 2u^2 F_{u^2}(u^2, \mathbf{x}). \quad (44)$$

When  $p(L_1) = p(M^{-1}L_1) = 1$  and  $\lambda$  is the single positive eigenvalue of  $M^{-1}L_1$  [i.e. Eq. (43)], it is easy to show using the spectral properties of Schrödinger operators that the corresponding eigenfunction  $\psi(\mathbf{x})$  is nodeless (a similar fact for the 1D case can be found in [32]). Since  $u(\mathbf{x})$  is also nodeless,  $\langle \psi, u \rangle \neq 0$ .

It is remarkable that the AITEM (16)-(18) can not only produce solitary waves, but also determine their linear stability properties. This is like “killing two birds with one stone”. To the authors’ knowledge, there are no other numerical methods for solitary waves which possess this same property. Note, however, that this property holds only for nodeless solitary waves. For solitary waves with nodes, this connection between convergence of the AITEM and linear stability of the solitary wave can break down.

## 5 Optimal acceleration of the imaginary-time evolution method

In the AITEM (16)-(18) for Eq. (4), a practical choice of the acceleration operator  $M$  is

$$M = c - \nabla^2, \quad c > 0. \quad (45)$$

The reason for this choice is two fold: first,  $M^{-1}$  is very easy to compute by the fast Fourier transform; second, all eigenvalues of  $\mathcal{L}$  are  $O(1)$ , which makes  $\Delta t_{max} = O(1)$  as well. For this  $M$ , an important question then is: at what value of  $c$  does the AITEM converge the fastest? We will answer this question in this section. Note that the use of a seemingly more general form of the

acceleration operator  $M = c_1 - c_2 \nabla^2$  is equivalent to (45) by a rescaling of the time step  $\Delta t$  in Eq. (17), and hence does not warrant consideration.

First, we quantify the convergence rate of the AITEM. From Eq. (23), we see that the error  $\tilde{u}_n$  evolves in proportion to  $R^n$ , where

$$R(c, \Delta t) = \max \{|1 + \Lambda_{min} \Delta t|, |1 + \Lambda_{max} \Delta t|\}, \quad (46)$$

and  $\Lambda_{min}(c)$ ,  $\Lambda_{max}(c)$  are the smallest and largest non-zero eigenvalues of Eq. (25). If  $R < 1$ , the AITEM converges, and vice versa. In this section, we assume that the AITEM converges (under the stepsize restriction in Theorem 1). This means that both  $\Lambda_{min}(c)$  and  $\Lambda_{max}(c)$  are negative. The parameter  $R$  characterizes the rate of convergence and will be called the convergence factor. Smaller  $R$  leads to faster convergence. For fixed  $c$ , it is seen from Eq. (46) that the smallest  $R$  is reached at

$$\Delta t = \Delta t_*(c) \equiv -\frac{2}{\Lambda_{min} + \Lambda_{max}}, \quad (47)$$

whence

$$R_*(c) \equiv R(c, \Delta t_*) = \frac{\Lambda_{min} - \Lambda_{max}}{\Lambda_{min} + \Lambda_{max}}. \quad (48)$$

The value of  $c$  which makes  $R_*(c)$  minimal gives optimal acceleration of the AITEM and will be denoted as  $c_{opt}$ . The determination of  $c_{opt}$  is the focus of this section.

Before analytically determining  $c_{opt}$ , we first present a numerical example. Consider the NLS equation (19) with  $\mu = 1$  again. For each  $c$  value in Eq. (45), we have numerically obtained  $\Lambda_{min}(c)$  and  $\Lambda_{max}(c)$  of operator  $\mathcal{L}$  by discretizing Eq. (25) and turning it into a matrix eigenvalue problem. The resulting  $R_*(c)$  function is then obtained from Eq. (48) and plotted in Fig. 3(a). We see that the minimum of  $R_*(c)$  occurs at  $c = 1$ , thus  $c_{opt} = 1$ . At this  $c$  value, dependence of the convergence factor  $R$  on the timestep  $\Delta t$  can be calculated from Eq. (46) and is displayed in Fig. 3(b). We see that when  $\Delta t > 2$ ,  $R > 1$ , thus iterations diverge. When  $0 < \Delta t < 2$ , iterations converge, and fastest convergence occurs when  $\Delta t \approx 1.51$ , which is the value from Eq. (47).

In the above numerical example, it is observed that  $c_{opt} = \mu$ . Is this a coincidence? The answer is negative. Below, we will show that for a large class of equations (4) with localized potentials,  $c_{opt} = \mu$ . This result is stated in the following theorem.

**Theorem 2** *Consider Eq. (4) with  $\lim_{|\mathbf{x}| \rightarrow \infty} F(0, \mathbf{x}) = 0$ . If  $\mathcal{V}(\mathbf{x})$  given in (44) does not change sign, then  $c_{opt} = \mu$  in the AITEM (16)-(18). If  $\mathcal{V}(\mathbf{x})$  changes sign, then  $c = \mu$  is not optimal in the generic case.*

The generic case will be defined later in Lemma 3. It is noted that when  $\lim_{|\mathbf{x}| \rightarrow \infty} F(0, \mathbf{x}) = 0$ ,  $\mu > 0$  for solitary waves in Eq. (4).

To facilitate the proof of Theorem 2, we first establish a few lemmas.

**Lemma 2** *If  $\lim_{|\mathbf{x}| \rightarrow \infty} F(0, \mathbf{x}) = 0$  in Eq. (4), then the continuous spectrum of operator  $\mathcal{L}$  in (25) is given by*

$$\begin{aligned} \Lambda &\in (-1, -\frac{\mu}{c}], \quad \text{for } c > \mu; \\ \Lambda &\in [-\frac{\mu}{c}, -1), \quad \text{for } c < \mu. \end{aligned} \quad (49)$$

Moreover, if  $(\Lambda, \Psi)$  is a discrete eigenmode of Eq. (25), then

$$0 < -\frac{1}{\Lambda} \frac{d\Lambda}{dc} = \frac{\langle \Psi, \Psi \rangle}{\langle \Psi, M\Psi \rangle} < \frac{1}{c}. \quad (50)$$

**Proof:** First, since  $\mathcal{L} \rightarrow M^{-1}L_1$  as  $\mathbf{x} \rightarrow \infty$ , the continuous spectrum of  $\mathcal{L}$  is then the same as that of  $M^{-1}L_1$ , which can be easily shown to be (49). Next, we consider how a discrete eigenvalue  $\Lambda$  changes with  $c$ . The eigenvalue equation  $\mathcal{L}\Psi = \Lambda\Psi$  can be rewritten as

$$L_1\Psi - Hu = \Lambda M\Psi, \quad (51)$$

where  $H = \langle L_1\Psi, M^{-1}u \rangle / \langle u, M^{-1}u \rangle$ . Differentiating Eq. (51) with respect to  $c$ , then taking its inner product with  $\Psi$  and noticing  $\Psi \in S$ , we get

$$\langle (L_1 - \Lambda M) \frac{\partial \Psi}{\partial c}, \Psi \rangle = \langle \frac{d\Lambda}{dc} M\Psi + \Lambda\Psi, \Psi \rangle. \quad (52)$$

Since both  $L_1$  and  $M$  are self-adjoint and utilizing Eq. (51), we have

$$\langle (L_1 - \Lambda M) \frac{\partial \Psi}{\partial c}, \Psi \rangle = \langle \frac{\partial \Psi}{\partial c}, (L_1 - \Lambda M)\Psi \rangle = H \langle \frac{\partial \Psi}{\partial c}, u \rangle = H \frac{d}{dc} \langle \Psi, u \rangle, \quad (53)$$

which is zero since  $\Psi \in S$ . Thus from Eq. (52), we get

$$-\frac{1}{\Lambda} \frac{d\Lambda}{dc} = \frac{\langle \Psi, \Psi \rangle}{\langle \Psi, M\Psi \rangle}. \quad (54)$$

Since  $\langle \Psi, M\Psi \rangle > c\langle \Psi, \Psi \rangle > 0$ , Lemma 2 is proved.  $\square$

**Lemma 3** *Consider Eq. (4) with  $\lim_{|\mathbf{x}| \rightarrow \infty} F(0, \mathbf{x}) = 0$ . If either  $\Lambda_{\min}(\mu) = -1$  or  $\Lambda_{\max}(\mu) = -1$ , then  $c_{\text{opt}} = \mu$ . If neither  $\Lambda_{\max}(\mu)$  nor  $\Lambda_{\min}(\mu)$  equals  $-1$ , then in the generic case where*

$$\frac{1}{\Lambda_{\max}} \frac{d\Lambda_{\max}}{dc} \Big|_{c=\mu} \neq \frac{1}{\Lambda_{\min}} \frac{d\Lambda_{\min}}{dc} \Big|_{c=\mu}, \quad (55)$$

$c = \mu$  is not optimal.

**Proof:** Differentiating formula (48) of  $R_*(c)$  with respect to  $c$ , one gets:

$$\frac{dR_*}{dc} = \frac{2\Lambda_{\min}\Lambda_{\max}}{(\Lambda_{\min} + \Lambda_{\max})^2} \left[ \frac{1}{\Lambda_{\min}} \frac{d\Lambda_{\min}}{dc} - \frac{1}{\Lambda_{\max}} \frac{d\Lambda_{\max}}{dc} \right]. \quad (56)$$

The factor in front of the square brackets above is positive since both  $\Lambda_{max}$  and  $\Lambda_{min}$  are negative (see beginning of this section). Following the assumption of this lemma, suppose, for definiteness, that  $\Lambda_{min}(\mu) = -1$ . When  $c$  decreases from  $\mu$ , the lower edge of the continuous spectrum decreases as  $-\mu/c$  [see Eq. (49)]. Due to inequality (50), all discrete eigenvalues of  $\mathcal{L}$  decrease slower than  $-\mu/c$ , thus  $\Lambda_{min}(c) = -\mu/c$ . Then using Eqs. (50) and (56) one obtains:

$$\frac{dR_*}{dc} < \left| \frac{2\Lambda_{min}\Lambda_{max}}{(\Lambda_{min} + \Lambda_{max})^2} \right| \left[ -\frac{c}{\mu} \frac{\mu}{c^2} + \frac{1}{c} \right] = 0, \quad c < \mu. \quad (57)$$

When  $c$  increases from  $\mu$ , the lower edge of the continuous spectrum is always at  $-1$  [see Eq. (49)], while discrete eigenvalues of  $\mathcal{L}$  all increase [see Eq. (50)], thus  $\Lambda_{min}(c) = -1$ . Then using Eqs. (50) and (56) we get

$$\frac{dR_*}{dc} > \left| \frac{2\Lambda_{min}\Lambda_{max}}{(\Lambda_{min} + \Lambda_{max})^2} \right| [0 + 0] = 0, \quad c > \mu. \quad (58)$$

Inequalities (57)–(58) mean that  $R_*(c)$  has a global minimum at  $c = \mu$ , thus  $c_{opt} = \mu$ . If  $\Lambda_{max}(\mu) = -1$ , following similar arguments one can show that  $c_{opt} = \mu$  as well.

If, however,  $\Lambda_{min}(\mu) < -1$  and  $\Lambda_{max}(\mu) > -1$ , then under the condition (55) which holds in the generic case,  $R'_*(\mu)$  exists and is not equal to zero. Thus the minimum of  $R_*(c)$  is not at  $c = \mu$ , i.e.  $c = \mu$  is not optimal. Lemma 3 is thus proved.  $\square$

In the following two lemmas, we establish the conditions under which either  $\Lambda_{min}(\mu) = -1$  or  $\Lambda_{max}(\mu) = -1$ . For convenience, we define  $M_0 \equiv M_{c=\mu} = \mu - \nabla^2$ ,  $\mathcal{L}_0 \equiv \mathcal{L}_{c=\mu}$ . Then  $\Lambda_{min}(\mu)$  and  $\Lambda_{max}(\mu)$  are the smallest and largest eigenvalues of  $\mathcal{L}_0$ .

**Lemma 4** *Suppose  $\lim_{|\mathbf{x}| \rightarrow \infty} F(0, \mathbf{x}) = 0$  in Eq. (4), then  $\mathcal{L}_0$  and  $M_0^{-1}L_1$  both do not have continuous spectrum, and their discrete eigenvalues accumulate at  $-1$ . In addition, if the smallest eigenvalue  $\lambda_{min}$  of  $M_0^{-1}L_1$  is  $-1$ , then  $\Lambda_{min}(\mu) = -1$ ; if  $M_0^{-1}L_1$  has two or more eigenvalues that are less than  $-1$ , then  $\Lambda_{min}(\mu) < -1$ . Similarly, if the largest eigenvalue  $\lambda_{max}$  of  $M_0^{-1}L_1$  is  $-1$ , then  $\Lambda_{max}(\mu) = -1$ ; if  $M_0^{-1}L_1$  has two or more eigenvalues greater than  $-1$ , then  $\Lambda_{max}(\mu) > -1$ .*

**Proof:** Operators  $M_0^{-1}L_1$  and  $\mathcal{L}_0$  do not have continuous eigenvalues, as follows from Eq. (49). The eigenvalue equation  $M_0^{-1}L_1\psi = \lambda\psi$  is the same as the Schrödinger equation (43). Using well known spectral properties of the Schrödinger operators, we know that operator  $M_0^{-1}L_1$  has an infinite number of (discrete) eigenvalues, which accumulate in such a way that  $(1 + \lambda)^{-1}$  approaches either  $+\infty$  or  $-\infty$ , or both (this fact for the 1D case can be found in [32]). Thus the accumulation point of eigenvalues for  $M_0^{-1}L_1$  is  $-1$ .

Applying the technique in the proof of Theorem 1 (see Eqs. (34)–(35), or [2, 21]) on the eigenvalue problem for  $\mathcal{L}_0$ , one can show that between every two adjacent eigenvalues of  $M_0^{-1}L_1$ , there is an eigenvalue of  $\mathcal{L}_0$ . Thus,  $-1$  is also an accumulation point of eigenvalues for  $\mathcal{L}_0$ . By the same reason, if the smallest eigenvalue  $\lambda_{min}$  for  $M_0^{-1}L_1$  is  $-1$ , then  $\Lambda_{min}(\mu) = -1$ ; if  $M_0^{-1}L_1$  has two or more eigenvalues that are less than  $-1$ , then  $\Lambda_{min}(\mu) < -1$ . Similarly, if the largest eigenvalue  $\lambda_{max}$  for  $M_0^{-1}L_1$  is  $-1$ , then  $\Lambda_{max}(\mu) = -1$ ; if  $M_0^{-1}L_1$  has two or more eigenvalues greater than  $-1$ , then  $\Lambda_{max}(\mu) > -1$ . Lemma 4 is thus proved.  $\square$

**Lemma 5** Consider Eq. (4) with  $\lim_{|\mathbf{x}| \rightarrow \infty} F(0, \mathbf{x}) = 0$ . For operator  $M_0^{-1}L_1$ , if  $\mathcal{V}(\mathbf{x}) \geq 0$  for all  $\mathbf{x}$ , then its smallest eigenvalue  $\lambda_{min}$  is  $-1$ ; if  $\mathcal{V}(\mathbf{x}) \leq 0$  for all  $\mathbf{x}$ , then its largest eigenvalue  $\lambda_{max}$  is  $-1$ ; if  $\mathcal{V}(\mathbf{x})$  changes sign, then there is an infinite number of its discrete eigenvalues on both sides of  $-1$ .

**Proof:** Consider the eigenvalue equation  $M_0^{-1}L_1\psi = \lambda\psi$ , which is the same as Eq. (43). Taking the inner product of Eq. (43) with  $\psi$ , we get

$$1 + \lambda = \frac{\langle \mathcal{V}\psi, \psi \rangle}{\langle M_0\psi, \psi \rangle}. \quad (59)$$

If  $\mathcal{V}(\mathbf{x}) \geq 0$  for all  $\mathbf{x}$ , then since  $M_0$  is a positive definite self-adjoint operator, the right hand side of the above equation is non-negative, thus  $\lambda > -1$ . Due to Lemma 4, eigenvalues of  $M_0^{-1}L_1$  accumulate at  $-1$ , thus  $\lambda_{min} = -1$ . By similar arguments, if  $\mathcal{V}(\mathbf{x}) \leq 0$  for all  $\mathbf{x}$ , then  $\lambda_{max} = -1$ . If  $\mathcal{V}(\mathbf{x})$  changes sign, then Eq. (43) has infinite numbers of discrete eigenvalues on both sides of  $-1$  [32]. Hence Lemma 5 is proved.  $\square$

With these lemmas, we are now ready to prove Theorem 2.

**Proof of Theorem 2:** If  $\mathcal{V}(\mathbf{x})$  does not change sign, then by Lemmas 4 and 5,  $\Lambda_{min}(\mu) = -1$  or  $\Lambda_{max}(\mu) = -1$ , hence by Lemma 3,  $c_{opt} = \mu$ . On the other hand, if  $\mathcal{V}(\mathbf{x})$  changes sign, Lemma 5 indicates that there are infinitely many eigenvalues of  $M_0^{-1}L_1$  both below and above  $-1$ . Then by Lemma 4, there are also infinitely many eigenvalues of  $\mathcal{L}_0$  both below and above  $-1$ , so that  $\Lambda_{min}(\mu) < -1$  and  $\Lambda_{max}(\mu) > -1$ . Then in the generic case defined by equation (55),  $c = \mu$  is not optimal by Lemma 3. Theorem 2 is thus proved.  $\square$

In practical implementations of the AITEM, after  $c_{opt} = \mu$  in Eq. (45) is chosen, one still needs to select the time step  $\Delta t$ . The best choice of  $\Delta t$  which leads to fastest convergence is given by Eq. (47). Since the exact values of  $\Lambda_{min}$  and  $\Lambda_{max}$  are usually not available, below we give the interval of values where the optimal time step can be found. When  $\mathcal{V}(\mathbf{x}) \geq 0$  for all  $\mathbf{x}$ ,  $\Lambda_{min}(\mu) = -1$ , and  $-1 < \Lambda_{max}(\mu) < 0$ , hence  $1 < \Delta t_*(\mu) < 2$ . When  $\mathcal{V}(\mathbf{x}) \leq 0$  for all  $\mathbf{x}$ ,  $\Lambda_{min}(\mu) < -1$  and  $\Lambda_{max}(\mu) = -1$ , hence  $\Delta t_*(\mu) < 1$ .

In some physical problems, the assumption  $\lim_{|\mathbf{x}| \rightarrow \infty} F(0, \mathbf{x}) = 0$  is not met, i.e. the potential in Eq. (4) is not localized. One example is the following type of equations

$$\nabla^2 u + V(\mathbf{x})u + G(u^2, \mathbf{x})u = \mu u, \quad (60)$$

where  $V(\mathbf{x})$  is a periodic function in  $\mathbf{x}$ , and  $G(0, \mathbf{x}) \rightarrow 0$  as  $\mathbf{x} \rightarrow \infty$ . For these equations, if we take the acceleration operator in the form of  $M = c - \nabla^2 - V(\mathbf{x})$ , then we can also show that under conditions analogous to those in Theorem 2,  $c_{opt} = \mu$ . However, for this form of  $M$ , it is not easy to compute  $M^{-1}$ . So in practice, it may still be better to use the simple form (45) for Eq. (60) instead. In that case,  $c_{opt}$  is not known analytically and may need to be estimated by trial and error (see Example 4 in Sec. 7). Our experience shows that in many cases, taking a suboptimal  $c$  does not slow down the method significantly as long as the  $c$  taken is not far away from  $c_{opt}$ . Thus using the form (45) of  $M$  for Eq. (60) does not constitute a significant disadvantage.



Lastly, we would like to point out that most of the results in Secs. 3, 4 and 5 can be extended to a wider class of equations

$$\mathcal{D}u + F(u^2, \mathbf{x})u = \mu u, \quad (61)$$

where  $u$  is a real-valued localized function,  $F$  is also real-valued,  $\mu$  is a real parameter, and  $\mathcal{D}$  is a general linear self-adjoint semi-negative-definite constant-coefficient pseudo-differential operator. The previous equation (4) is a special case of (61) with  $\mathcal{D} = \nabla^2$ . For this general equation (61), the AITEM is still (16)-(18), with  $\nabla^2$  replaced by  $\mathcal{D}$ . The convergence conditions of this AITEM are still the same as those in Theorem 1, except that  $\nabla^2$  in the definition (14) of  $L_1$  is replaced by  $\mathcal{D}$ . Regarding optimal acceleration, if  $M = c - \mathcal{D}$  is taken, then we can also show that  $c_{opt} = \mu$  when  $\lim_{|\mathbf{x}| \rightarrow \infty} F(0, \mathbf{x}) = 0$  and  $\mathcal{V}(\mathbf{x})$  as defined in (44) does not change sign. The connection between convergence of the AITEM and linear stability of a nodeless solitary wave can also be extended to other types of nonlinear wave equations. For instance, consider the generalized one-dimensional Korteweg de Vries (KdV) equation

$$U_t + [\mathcal{D}U + F(U^2)U]_x = 0, \quad (62)$$

where  $U(x, t)$  and  $F(\cdot)$  are both real-valued functions,  $F(0) = 0$ , and  $\mathcal{D}$  is a general linear self-adjoint semi-negative-definite constant-coefficient pseudo-differential operator. Looking for moving solitary waves of the form  $U(x, t) = u(x - \mu t)$ , where  $\mu$  is a real parameter, we get an equation for  $u$  which is a special form of (61). For Eq. (62), it has been shown that if  $u(x)$  has no nodes and  $p(L_1) = 1$ , then the solitary wave  $u(x - \mu t)$  is linearly stable if  $P'(\mu) > 0$  and linearly unstable if  $P'(\mu) < 0$  [33, 34]. In this case, for generic acceleration operators  $M$  where the eigenfunction of  $M^{-1}L_1$ 's positive eigenvalue is non-orthogonal to  $u(x)$ , the convergence conditions of the AITEM in Theorem 1 are the same as the stability conditions above. Thus the connection between convergence of the AITEM and linear stability of the solitary wave holds for Eq. (62) as well.

## 6 The accelerated imaginary-time evolution method with amplitude normalization

The AITEM (16)-(18) discussed above employed the power normalization [see (16)], which has commonly been used in all previous ITEM-type methods. A consequence of this normalization is that when  $P'(\mu) = 0$ , this method is doomed to fail. In certain cases when  $P'(\mu) < 0$  (see case 2 in Theorem 1), this AITEM diverges as well. In this section, we will propose a different normalization for the AITEM which can overcome the above difficulties.

This new normalization is the amplitude normalization. In other words, instead of fixing the power of the solution we are seeking, we fix the amplitude of  $u(\mathbf{x})$  (i.e., the largest value of  $|u(\mathbf{x})|$ ). Thus, this new AITEM we propose for Eq. (4) is

$$u_{n+1} = \frac{A}{|\hat{u}_{n+1}|_{max}} \hat{u}_{n+1}, \quad (63)$$

$$\hat{u}_{n+1} = u_n + M^{-1} (L_{00}u - \mu u)_{u=u_n, \mu=\mu_n} \Delta t, \quad (64)$$

and

$$\mu_n = \frac{\langle L_{00}u, M^{-1}u \rangle}{\langle u, M^{-1}u \rangle} \Big|_{u=u_n}, \quad (65)$$

where  $A = |u|_{max}$  is the pre-specified amplitude of  $u(\mathbf{x})$ . This AITEM with amplitude normalization, which we denote as AITEM(A.N.), can converge regardless of the value of  $P'(\mu)$ .

We have tested this AITEM(A.N.) on various examples, and found that it is almost always more superior than the first AITEM (16)-(18). This superiority is reflected on two aspects: (i) in cases where the first AITEM does not converge, the AITEM (A.N.) often can converge; (ii) in cases where the first AITEM converges, the AITEM(A.N.) often converges faster.

To illustrate the first aspect of the AITEM (A.N.) superiority, we consider the following example.

**Example 3.** The 2D NLS equation

$$u_{xx} + u_{yy} + u^3 = \mu u \quad (66)$$

admits a family of single-hump (fundamental) solitary waves, all of which have the same power  $P = 11.70$ . Since  $P'(\mu) = 0$  everywhere, the first AITEM (16)-(18) clearly can not converge to these solitary waves. However, the AITEM (A.N.) can not only converge, but also converge very fast. To illustrate, we select the solitary wave with amplitude  $A = 1$ , whose corresponding propagation constant is  $\mu = 0.2054$ . This solitary wave is displayed in Fig. 4(a). We take the acceleration operator  $M$  as (45), the initial guess as a Gaussian hump  $u_0(x, y) = e^{-(x^2+y^2)/10}$ , the spatial domain as a square with side length of 30, with each dimension discretized by 128 points. We also take  $(c, \Delta t) = (0.5, 1)$ , which is nearly optimal. With these choices, the AITEM (A.N.) rapidly converges to the solitary wave [see the error diagram in Fig. 4(b)]. Indeed, it takes only 27 iterations for the error to fall below  $10^{-10}$ . For comparison, we applied the standard Petviashvili method to this example [11], taking the same spatial discretizations and initial condition as above. The error diagram of the Petviashvili method is also displayed in Fig. 4(b). We see that the AITEM (A.N.) is faster than the Petviashvili method by about 40%.

The second aspect of the AITEM (A.N.) superiority over the first AITEM will be illustrated by examples in the next section.

It should be pointed out that for the AITEM (A.N.), the connection between convergence of the scheme and linear stability of the solitary wave disappears. Regarding its convergence conditions, this question can be analyzed by techniques similar to those used in Secs. 3 and 5. This will not be done in this article, and will be left for future studies.

## 7 Examples illustrating convergence rates of the AITEMs

In this section, we will apply the two proposed AITEMs (16)-(18) and (63)-(65) to two physical examples, and compare their convergence speeds. In addition, we will compare them to the

Petviashvili method whenever applicable.

**Example 4** Let us first consider a 2D NLS equation with a periodic potential,

$$u_{xx} + u_{yy} + V_0 (\cos^2 x + \cos^2 y) u + u^3 = \mu u, \quad (67)$$

which has recently attracted much interest due to its application to optical lattices and Bose-Einstein condensates [3, 35, 36]. This equation admits a family of nodeless solitary waves. One of them with  $V_0 = 3$ ,  $P = 3$ ,  $\mu = 3.7045$  and amplitude  $A = 1.0384$  is displayed in Fig. 5 (a). For this wave,  $p(L_1) = 1$  and  $P'(\mu) > 0$ , thus the AITEM converges for generic choices of  $M$ . We applied the AITEM and AITEM(A.N.) to search for this solitary wave. The acceleration operator  $M$  was taken as (45), the spatial domain taken to be a square with side length of  $10\pi$ , with each dimension discretized by 128 points. As the initial guess, we took a Gaussian profile  $u_0(x, y) = \exp(-x^2 - y^2)$ . For our choice of (45),  $c_{opt}$  is not known analytically. Hence we scanned values of  $c$  and  $\Delta t$  in the AITEMs and found that taking  $c = 0.7$  and  $\Delta t = 1$  yielded the fastest (or nearly fastest) convergence for both AITEM and AITEM(A.N.). The error diagrams versus the iteration number for these two methods are shown in Fig. 5(b). We see that an error below  $10^{-10}$  is reached by the AITEM and AITEM(A.N.) in about 310 and 130 iterations respectively. Thus the AITEM (A.N.) converges much faster than the AITEM. In the appendix, the matlab code of AITEM(A.N.) on this example is attached, so that the reader can test this method themselves. For Eq. (67), the original Petviashvili method does not apply [11]. Several generalizations of that method for equations such as (67) have been proposed recently [13, 14, 37]. A comparison between those generalized Petviashvili methods and the AITEMs in this paper will be considered elsewhere.

**Example 5** Another example we consider is an equation whose linear part is not of the Schrödinger type. Specifically, we consider the integrable Kadomtsev-Petviashvili (KP) equation, whose stationary solutions satisfy the equation

$$u_{xx} - \partial_x^{-2} u_{yy} + u^n = \mu u, \quad n = 2 \quad (68)$$

and the constraint

$$\int_{-\infty}^{\infty} u(x, y) dy = 0. \quad (69)$$

The analytical expression for solitary waves of Eq. (68) is [38]

$$u = 12\mu \frac{3 + \mu^2 y^2 - \mu x^2}{(3 + \mu^2 y^2 + \mu x^2)^2}, \quad (70)$$

and their power function is  $P(\mu) = 24\pi\sqrt{\mu}$ . It is known that  $p(L_1) = 1$  for solutions (70) [12], and  $P'(\mu) > 0$  in view of the above power formula. Thus the AITEM converges to these localized solutions for generic choices of  $M$  (see end of Sec. 5). We applied the AITEM, AITEM (A.N.) and the Petviashvili method [11] to compute one of these solutions with  $\mu = 1$ , whose profile is shown in Fig. 6(a). The spatial domain was taken as a square with side length of 120, discretized by 512 points in each dimension. The acceleration operator  $M$  in the AITEMs was taken as  $M = c - \partial_{xx} + \partial_x^{-2} \partial_{yy}$ . Since  $\mathcal{V}(x, y) = 2u$  changes sign here, generically  $c_{opt} \neq \mu$  in the AITEM. For the AITEM and AITEM (A.N.), we took  $(c, \Delta t) = (1.4, 1.7)$  and  $(1.4, 1.4)$  respectively, which yield near-optimal convergence for the underlying methods. For all three methods, we imposed

the constraint (69) by setting the coefficient of the  $\mathbf{k}_x = 0$  Fourier harmonic to be zero at every iteration. The error diagrams for these methods are displayed in Fig. 6(b). This time, an error below  $10^{-10}$  is reached by the AITEM, AITEM(A.N.) and the Petviashvili method in about 140, 40 and 90 iterations respectively. Thus the AITEM (A.N.) converges much faster than the Petviashvili method, while the Petviashvili method converges faster than the AITEM.

We have studied solitary waves in the generalized KP equation (68) (with  $n \neq 2$ ) as well. In those equations, if  $n > 7/3$ , solitary waves are unstable [39]. In such cases, we found that the AITEM (16)-(18) diverged. Thus the connection between convergence of that AITEM and the stability of the underlying solitary wave holds for the generalized KP equation as well.

From the above examples, we conclude that the AITEM (A.N.) converges faster than the AITEM and Petviashvili methods, while the AITEM and the Petviashvili method are comparable in convergence speeds.

Before concluding the paper, we make a comment on the practical implementations of the AITEMs (and other methods such as the Petviashvili method as well). If the convergence theorem predicts that a method diverges for a solitary wave, sometimes iterations can still converge (at least to a certain accuracy). This can happen, for instance, when the iteration operator  $\mathcal{L}$  has a single unstable symmetric eigenmode, but the initial condition is chosen to be, and the final solution is, strictly anti-symmetric. In that case, the unstable symmetric eigenmode may not yet be excited before the iterations have already converged. Such an example is Eq. (42), which admits anti-symmetric solitary waves. When  $P = 3$  (see Fig. 2),  $p(L_1) = 1$ , and  $P'(3) < 0$ . Hence the AITEM (16)-(18) should diverge. However, we found that if we used anti-symmetric initial conditions, then the AITEM iterations can converge to the solution with error below  $10^{-12}$ . However, if a small symmetric component was introduced into the initial condition, the iterations would diverge. Thus, the convergence results obtained in this paper must be understood as pertaining to generic initial conditions. If non-generic initial conditions are used in practical implementations of the AITEMs, better convergence behavior may be observed.

## 8 Summary

In this paper, we proposed two accelerated imaginary-time evolution methods for computations of solitary waves in arbitrary spatial dimensions. The first method is the AITEM (16)-(18) with the conventional power normalization. For this method, the convergence conditions were derived. These conditions show that this method usually converges to nodeless solutions, but there also exist cases when this AITEM converges to solitary waves with nodes. For nodeless solutions, we also showed that this AITEM converges if and only if the solitary wave is linearly stable. Conditions for optimal accelerations of this AITEM were also derived. The second method we proposed is the AITEM (A.N.) (63)-(65) which employs a novel amplitude normalization. Both methods were applied to several examples of physical interest, and we found that the AITEM (A.N.) delivers the best performance, while the AITEM and the Petviashvili method are comparable in performance.

## Acknowledgment

The work of J.Y. is supported in part by The Air Force Office of Scientific Research under grant USAF 9550-05-1-0379, and the work of T.I.L. is supported in part by the National Science Foundation under grant DMS-0507429.

## Appendix: Matlab code of AITEM (A.N.) for Example 4

```
Lx=10*pi; Ly=10*pi; N=128; c=0.7; DT=1;
max_iteration=10000; error_tolerance=1e-10;

dx=Lx/N; x=-Lx/2:dx:Lx/2-dx; kx=[0:N/2-1 -N/2:-1]*2*pi/Lx;
dy=Ly/N; y=-Ly/2:dy:Ly/2-dy; ky=[0:N/2-1 -N/2:-1]*2*pi/Ly;
[X,Y]=meshgrid(x, y); [KX,KY]=meshgrid(kx, ky);

A=1.0384;
U=exp(-(X.^2+Y.^2)); U=U/max(max(abs(U)))*A;
for nn=1:max_iteration
    Uold=U;
    L00U=ifft2(-(KX.^2+KY.^2).*fft2(U))+3*(cos(X).^2+cos(Y).^2).*U + U.^3;
    MinvU=ifft2(fft2(U)./(c+KX.^2+KY.^2));
    mu=sum(sum(L00U.*MinvU))/sum(sum(U.*MinvU));
    U=U+ifft2(fft2(L00U-mu*U)./(KX.^2+KY.^2+c))*DT;
    U=U/max(max(abs(U)))*A;
    Uerror(nn)=sqrt(sum(sum(abs(U-Uold).^2))*dx*dy); Uerror(nn)
    if Uerror(nn) < error_tolerance
        break
    end
end
end
```

This code as well as Matlab codes for other examples can be downloaded at [www.cems.uvm.edu/~jyang/Publication.htm](http://www.cems.uvm.edu/~jyang/Publication.htm)

## References

- [1] N.K. Efremidis, S. Sears, D.N. Christodoulides, J.W. Fleischer and M. Segev, “Discrete solitons in photorefractive optically induced photonic lattices,” *Phys. Rev. E* **66**, 046602 (2002).
- [2] Y.S. Kivshar and G.P. Agrawal, *Optical solitons: from fibers to photonic crystals*, Academic Press, San Diego, 2003.

- [3] J. Yang and Z. Musslimani, “Fundamental and vortex solitons in a two-dimensional optical lattice,” *Opt. Lett.* **28**, 2094 (2003).
- [4] Th. Busch and J.R. Anglin, “Mössbauer effect for dark solitons in Bose-Einstein condensates,” <http://arxiv.org>, Preprint cond-mat 9809408.
- [5] M.L. Chiofalo, S.Succi, and M.P. Tosi, “Ground state of trapped interacting Bose-Einstein condensates by an explicit imaginary-time algorithm,” *Phys. Rev. E* **62**, 7438 (2000).
- [6] L.D. Carr and Y. Castin, “Dynamics of matter-wave bright soliton in an expulsive potential,” *Phys. Rev. A* **66**, 063602 (2002).
- [7] H.B. Keller, “Numerical solution of bifurcation and nonlinear eigenvalue problems,” in P. H. Rabinowitz, ed., *Applications of Bifurcation Theory*, pp. 359-384; Academic Press,
- [8] J.P. Boyd, “Why Newton’s Method is Hard for Travelling Waves: Small Denominators, KAM Theory, Arnold’s Linear Fourier Problem, Non-Uniqueness, Constraints and Erratic Failure,” *Math. Comput. Simul.* **74**, 7281 (2007).
- [9] J. Yang, “Internal oscillations and instability characteristics of (2+1) dimensional solitons in a saturable nonlinear medium,” *Phys. Rev. E* **66**, 026601 (2002).
- [10] P.G. Kevrekidis, K.O. Rasmussen, and A.R. Bishop, “Localized excitations and their thresholds,” *Phys. Rev. E* **61**, 4652 (2000).
- [11] V. I. Petviashvili, “Equation of an extraordinary soliton,” *Plasma Physics*, **2**, 469, (1976).
- [12] D.E. Pelinovsky and Yu. A. Stepanyants, “Convergence of Petviashvili’s iteration method for numerical approximation of stationary solutions of nonlinear wave equations,” *SIAM J. Numer. Anal.* **42**, 1110 (2004).
- [13] M.J. Ablowitz, Z.H. Musslimani, “Spectral renormalization method for computing self-localized solutions to nonlinear systems”, *Opt. Lett.* **30**, 21402142 (2005).
- [14] T.I. Lakoba and J. Yang, “A generalized Petviashvili iteration method for scalar and vector Hamiltonian equations with arbitrary form of nonlinearity”, *J. Comp. Phys.* **226**, 1668-1692 (2007).
- [15] J.J. Garcia-Ripoll and V.M. Perez-Garcia, “Optimizing Schrödinger functionals using Sobolev gradients: Applications to quantum mechanics and nonlinear optics,” *SIAM J. Sci. Comput.* **23**, 1316 (2001).
- [16] W. Bao and Q. Du, “Computing the ground state solution of Bose-Einstein condensates by a normalized gradient flow,” *SIAM J. Sci. Comput.* **25**, 1674 (2004).
- [17] V.S. Shchesnovich and S.B. Cavalcanti, “Rayleigh functional for nonlinear systems,” available at <http://www.arXiv.org>, Preprint nlin.PS/0411033.
- [18] J. Yang and T.I. Lakoba, “Universally-convergent squared-operator iteration methods for solitary waves in general nonlinear wave equations”, *Stud. Appl. Math.* **118**, 153-197 (2007).

- [19] J. Douglas and H.H. Rachford, “On the numerical solution of heat conduction problems in two and three space variables,” *Trans. Amer. Math. Soc.* **82**, 421 (1956).
- [20] S.E. Koonin, *Computational Physics*, Sec. 7.4; Addison-Wesley, Redwood City, 1986.
- [21] N. G. Vakhitov and A. A. Kolokolov, “Stationary solutions of the wave equation in the medium with nonlinearity saturation,” *Izv. Vyssh. Uchebn. Zaved. Radiofiz.* **16**, 1020 (1973) [*Radiophys. Quantum Electron.* **16**, 783 (1973)].
- [22] C. K. R. T. Jones, “Instability of standing waves for nonlinear Schrödinger-type equations, *Ergod. Theory Dynam. Syst.* **8**, 119 (1988).
- [23] M. Grillakis, “Linearized instability for nonlinear Schrödinger and Klein-Gordon equations,” *Comm. Pure Appl. Math.* **41**, 747 (1988).
- [24] M. Weinstein, “Lyapunov stability of ground states of nonlinear dispersive evolution equations,” *Comm. Pure Appl. Math.* **39**, 51 (1986).
- [25] W.A. Strauss, M. Grillakis, J. Shatah, W. Strauss, “Stability theory of solitary waves in the presence of symmetry. I”, *J. Funct. Anal.* **74**, 160C197 (1987).
- [26] W.A. Strauss, “Existence of solitary waves in higher dimensions,” *Comm. Math. Phys.* **55**, 149 (1977).
- [27] H. Berestycki and P.L. Lions, “Nonlinear scalar field equations I — Existence of a ground state,” *Arch. Rat. Mech. Anal.* **82**, 313 (1983).
- [28] J. Yang and Z. Chen, “Defect solitons in photonic lattices,” *Phys. Rev. E.* **73**, 026609 (2006).
- [29] R. Horn and C. Johnson, *Matrix Analysis*, Cambridge University Press, New York, 1991.
- [30] M. Struwe, *Variational Methods: Applications to Nonlinear Partial Differential Equations and Hamiltonian Systems*, 3rd ed., Springer, 2000. [Specifically, see the paragraph just below Theorem B.4 on page 246.]
- [31] W.A. Strauss, *Nonlinear Wave Equations*, CBMS Reg. Conf. Ser. Math, vol.73, AMS, Providence, RI, 1989.
- [32] E.L. Ince, *Ordinary differential equations*, Dover, New York, 1956. [Specifically, see the Theorem stated at the end of Sec. 10.61.]
- [33] J. L. Bona, P. E. Souganidis, and W. A. Strauss, “Stability and instability of solitary waves of Korteweg-de Vries type,” *Proc. Roy. Soc. London Ser. A* **411**, 395 (1987).
- [34] R. L. Pego and M. I. Weinstein, “Eigenvalues, and instabilities of solitary waves,” *Phil. Trans. Roy. Soc. London Ser. A* **340**, 47 (1992).
- [35] E.A. Ostrovskaya and Y.S. Kivshar, “Photonic crystals for matter waves: Bose-Einstein condensates in optical lattices,” *Optics Express* **12**, 19 (2004).
- [36] N.K. Efremidis, J. Hudock, D.N. Christodoulides, J.W. Fleischer, O. Cohen, and M. Segev, “Two-Dimensional Optical Lattice Solitons,” *Phys. Rev. Lett.* **91**, 213906 (2003).

- [37] Z. Musslimani and J. Yang, “Self-trapping of light in a two-dimensional periodic structure,” *J. Opt. Soc. Am. B.* **21**, 973 (2004).
- [38] S.V. Manakov, V.E. Zakharov, L.A. Bordag, A.R. Its, and V.B. Matveev, “Two-dimensional solitons of the Kadomtsev-Petviashvili equation and their interaction,” *Phys. Lett. A* **63**, 205 (1977).
- [39] X.P. Wang, M.J. Ablowitz, and H. Segur, “Wave collapse and instability of solitary waves of a generalized Kadomtsev-Petviashvili equation,” *Physica D* **78**, 241 (1994)



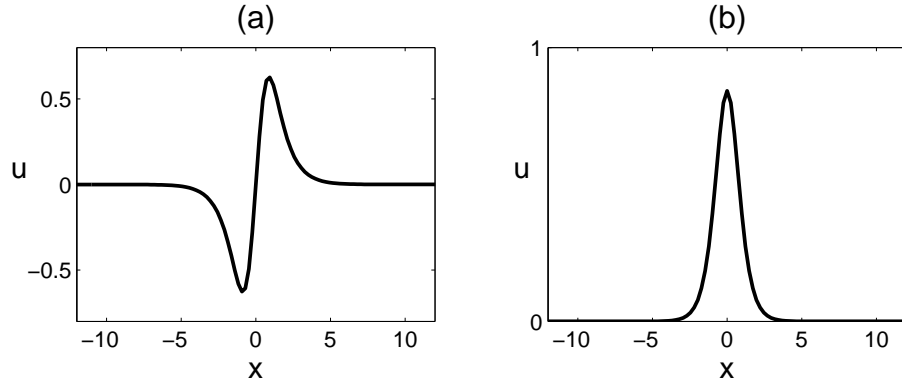


Figure 1: (a) A solitary wave with nodes in the focusing nonlinear Schrödinger equation (40) ( $\mu = 1.2689, P = 1$ ), for which the AITEM (16)-(18) diverges for any  $\Delta t$ ; (b) A nodeless solitary wave in the defocusing nonlinear Schrödinger equation (41) ( $\mu = 3.5069, P = 1$ ), for which the AITEM (16)-(18) converges if the stepsize condition  $\Delta t < \Delta t_{max}$  in Theorem 1 is met.

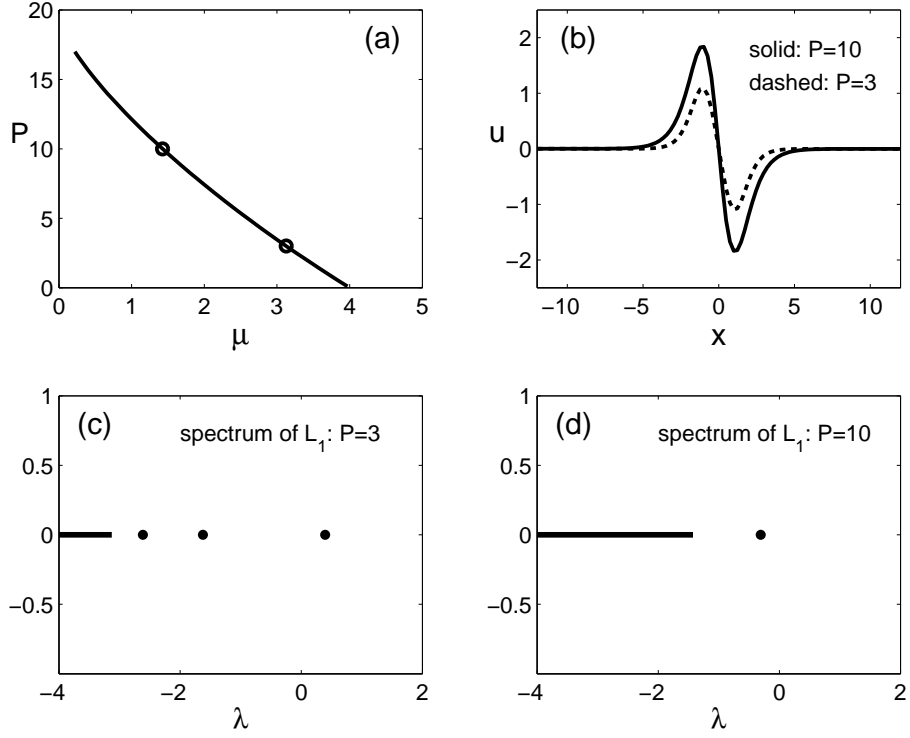


Figure 2: Solitary waves with nodes in the defocusing nonlinear Schrödinger equation (42) and their  $L_1$  spectra. (a) The power diagram; (b) two solitary waves with powers  $P = 3$  and  $10$ ; (c, d) spectra of  $L_1$  for these two waves. The AITEM (16)-(18) converges for the one with  $P = 10$  when the stepsize restriction in Theorem 1 is met.

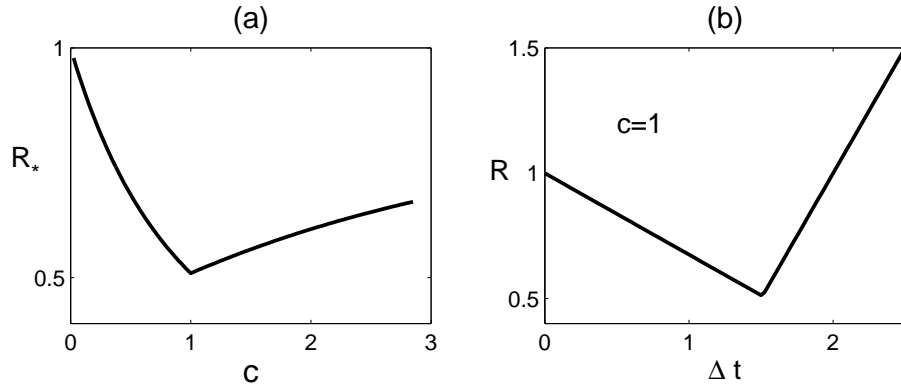


Figure 3: Convergence rates of the AITEM (16)-(18) for the NLS equation (19) with  $\mu = 1$ : (a) graph of the convergence factor  $R_*(c)$ ; (b) graph of  $R(\Delta t; c = 1)$  versus  $\Delta t$ .

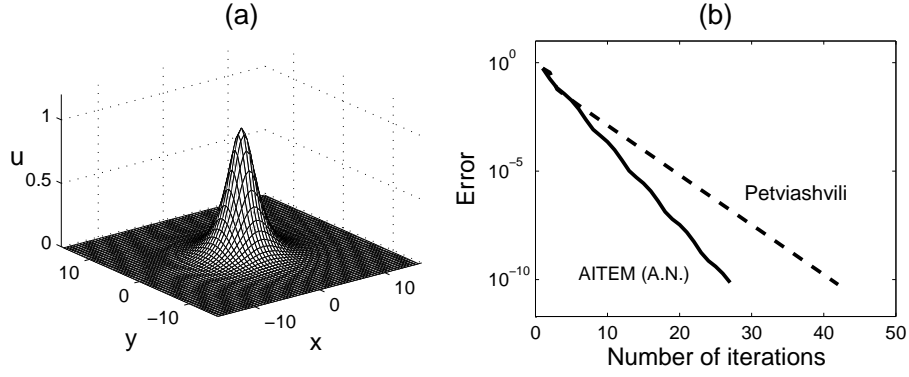


Figure 4: (a) A solitary wave in the two-dimensional NLS equation (66) with amplitude one; (b) error diagrams of the AITEM (A.N.) and the Petviashvili method for this solitary wave.

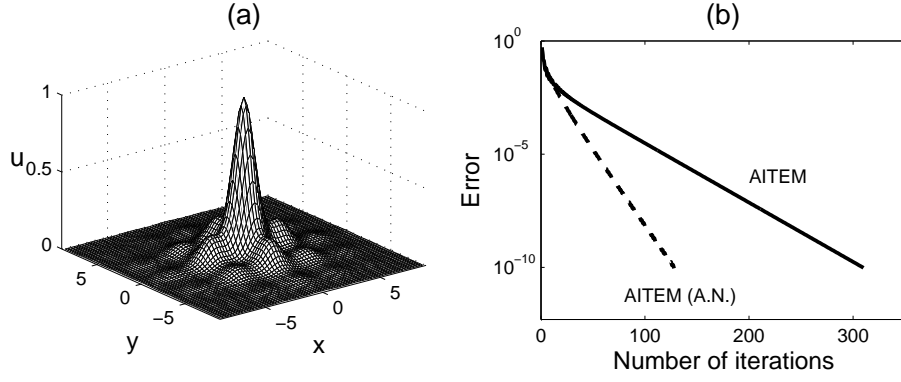


Figure 5: (a) A solitary wave in Eq. (67) with  $V_0 = 3$  and  $P = 3$ . (b) Error diagrams of the AITEM and AITEM (A.N.) [both with  $c = 0.7$ ,  $\Delta t = 1$ ] for this solitary wave.

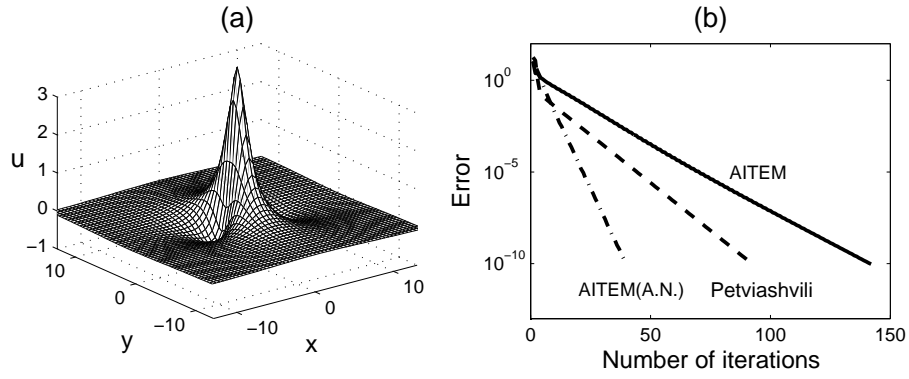


Figure 6: (a) A solitary wave in the KP equation (68) with  $\mu = 1$ ; (b) error diagrams of the AITEM (with  $c = 1.4, \Delta t = 1.7$ ), AITEM (A.N.) (with  $c = 1.4, \Delta t = 1.4$ ) and the Petviashvili method for this solitary wave.